Stanford Exploration Project, Report 75, November 17, 1997, pages 25–41

Plumes: Response of time migration to lateral velocity variation

James L. Black, Dimitri Bevc, Matt A. Brzostowski, Lewei Mo, Gopal Palacharla[1]

keywords: *velocity, time migration*

ABSTRACT

Lateral velocity variation causes time migration to misposition events. Black and Brzostowski (1993) quantify this error by developing a first order theory for the positioning error in terms of `x` and `t`. The response of a point diffractor in a medium with a simple lateral velocity variation is a distinctive cusp-like shape that we call a "plume". The nature of the plume is revealed by making two geometrical constructions based upon point diffractor ray-tracing: superposition of semicircles and summation along hyperbolas. The plume shapes derived by these two techniques are consistent with results obtained by migrating synthetic point diffractors using the Kirchhoff, Stolt, and Gazdag time migration methods. The shapes of these plumes resemble those predicted by Black and Brzostowski's simple first-order theory, but the actual plumes are less symmetric than the predictions. Thus a higher-order theory is needed.

INTRODUCTION

Time migration algorithms do not yield the correct image when velocity varies laterally. The correct image is best obtained by prestack depth migration. By studying the errors in time migration, it may be possible to link time migration with depth migration. This is desirable since time migration algorithms are generally robust, well understood and much less expensive than prestack depth migration.

Hubral (1977) argued that the image ray connects time migration with depth migration. He started with the incorrect assumption that time migration moves an event to the apex of the *true-diffraction curve*, the zero-offset response to a point diffractor. The apex of the *true-diffraction curve* is located at the end of the image ray, the ray that strikes the earth's surface at normal incidence. Since the image ray connects the top of the *true-diffraction curve* with the subsurface point, Hubral claimed that the image ray is the connection between time and depth migration. A correction method based on this view of the image ray can be applied to time migrated

[1]**email:** not available

data (Larner et al., 1981; Hatton et al., 1981).

This argument and correction is valid for events with small dips but fails for steeply dipping events. This failure is due to the fact that time migration moves an event to the apex of a *time migration curve* which is not the same as the *true-diffraction curve* for a medium with lateral velocity variation (Black and Brzostowski, 1993).

In this paper we study the effect of lateral velocity gradients on two dimensional zero-offset time migration. We use a simple dipping-layer earth model with an implicit velocity gradient. The main point of this paper is to derive the response of time migration to a point diffractor in a `v(x)` medium. We show that the response of time migration in a `v(x)` medium is a cusp-like shape that we call a "plume." Although we devote a great deal of attention to the exact nature of the plume, its existence is not a new discovery since examples of plumes can be found in Yilmaz's chapter on depth migration (Yilmaz, 1987). The shape and location of the plume is not as simple as predicted by Black and Brzostowski's first-order theory, but it can be explained using ray-tracing and geometrical constructions.

GEOMETRICAL CONSTRUCTION OF PLUMES

Dipping-Layer Model

The model used in this paper is displayed in Figure 1. An implicit velocity gradient is caused by the dipping layer since the velocity changes across it. We begin our study by analyzing the response of a point diffractor positioned below the layer. The parameters of the model were chosen to match the synthetic data example given by Black and Brzostowski (1993). The point diffractor is positioned at a depth of 4 kft at a horizontal position of 8 kft.

The *true-diffraction curve* for this model is the zero-offset response to a point diffractor. Ray-tracing with equations (A-4) and (A-5) of the Appendix shows that this curve is asymmetric (Figure 2). The arrival times are later where the low velocity wedge is thicker and earlier where the wedge is thinner. The apex of the curve is offset to the right of the diffractor position.

Semicircle Superposition

Time migration may be thought of as hyperbola summation or semi-circle superposition (Schneider, 1978). In order to illustrate the kinematics of time migration when there are lateral velocity variations, we first superimpose time migration semi-circles along the diffraction curve of Figure 2. This geometrical construction is shown in Figure 3, where the radius of each circle is determined by the RMS velocity that would be derived from a well drilled straight down to the diffractor from the surface at the diffractor location. This value is 8.846 kft/sec and is what we call as the well

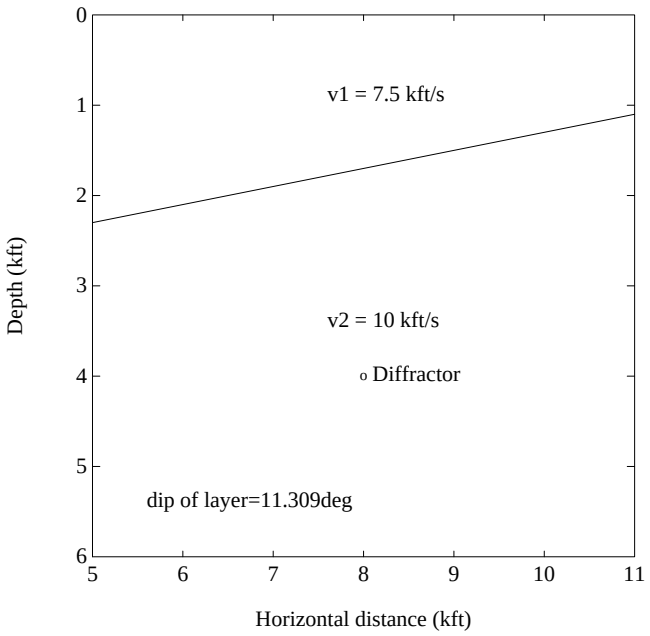

Figure 1: Dipping-layer model. The change in velocity across the dipping layer causes an implicit velocity gradient which depends on the dip of the layer. dimitri1-gem1 [NR]

RMS velocity. This is the migration velocity used throughout this paper. The points where the semi-circles add constructively form the time-migrated image of the point diffractor. Figure 4 is an enlarged view showing the semi-circle superposition near the apex of the *true-diffraction curve*. The envelope of semi-circles is displaced to the right of the true diffractor position at 8 kft and forms a distinctive cusp shape that opens to the right. This shape is what we call the "plume." The plume shows that the various dip components of a point diffractor end up at different positions on the time-migrated image. Thus the plume clearly shows that mis-focusing occurs when time migration is applied to a medium with lateral velocity variations.

The plume shape can be qualitatively explained by examining the kinematics of time migration. For the left side of the *true-diffraction curve* the migration velocity is too fast, so that limb of the curve is overmigrated. For the right side of the *true-diffraction curve* the migration velocity is too slow, so that limb of the curve is undermigrated.

Hyperbola Summation

The semi-circle superposition method allows us to visualize how the plume is built up from constructive interference. It does not, however, offer a convenient way to numerically compute the actual shape of the plume. A more effective way to compute

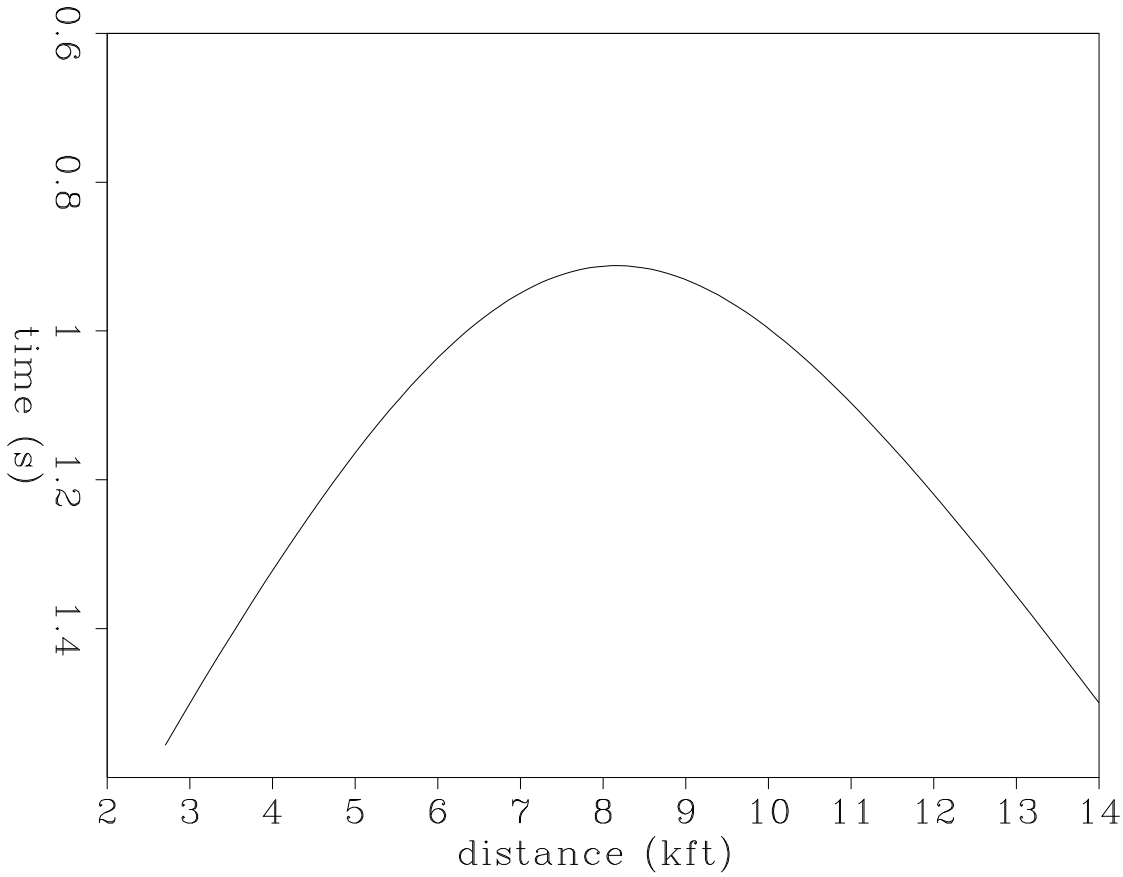

Figure 2: The *true-diffraction curve* for the dipping-layer model is an asymmetric curve. The apex of the curve is offset to the right and arrival times are later on the left than on the right because the low velocity wedge is thicker on the left. dimitri1-truedif [ER]

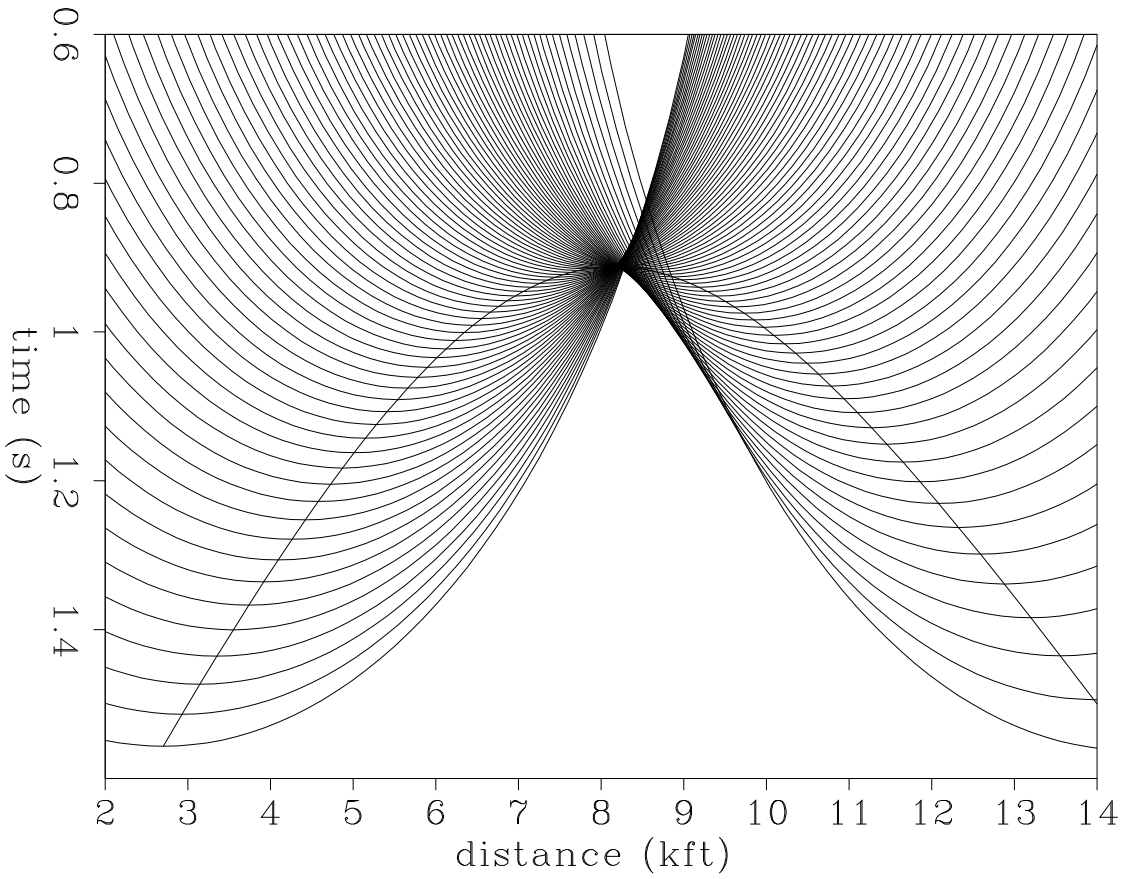

Figure 3: Time migration semi-circles are superimposed on the *true-diffraction curve* for the dipping-layer model. The points where the semi-circles add constructively form the migrated image. dimitri1-plmconstr [ER]

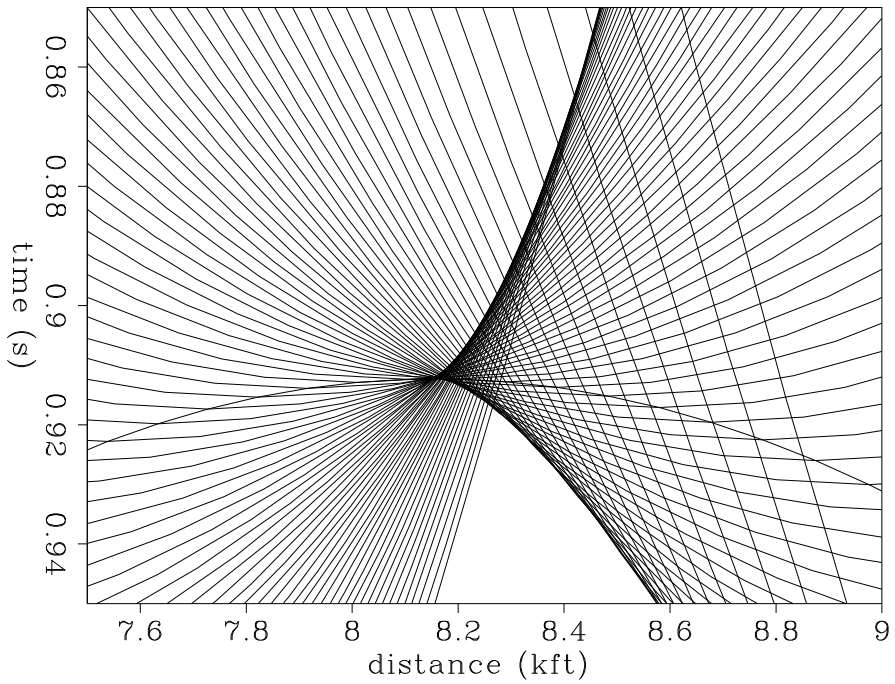

Figure 4: A close up of the time migration semi-circles superimposed along the *true-diffraction curve* near the apex of the *true-diffraction curve*. The envelope of semi-circles forms a plume. dimitri1-plmzoom [ER]

the time-migration response to a point diffractor is by summing along hyperbolas (Schneider, 1978). The analytical technique for summing along hyperbolas is called the "common- tangent" construction. It relies on the fact that the main contribution to the sum comes from the place where a time-migration hyperbola is tangent to the *true-diffraction curve* of Figure 2. The event at the tangency point is positioned by time migration to the apex of the time-migration hyperbola.

The time migration hyperbola is given by:

$$t_0^2 = t_k^2 + 4[\frac{x_0 - x_k}{V(x_m, t_m)}]^2 \tag{1}$$

Matching the slope of the hyperbola given by equation(1) with the time dip D of the event leads to the following formulas for the position of the time migrated point (x_k, t_k):

$$x_k = x_0 - [\frac{V(x_m, t_m)D}{2}][\frac{V(x_m, t_m)t_0}{2}] \tag{2}$$

$$t_k = t_0\sqrt{1 - [\frac{V(x_m, t_m)D}{2}]^2} \tag{3}$$

where

$$D = \frac{\partial t_0}{\partial x_0}$$

is the apparent time dip of the event to be migrated and $V(x_m, t_m)$ is the RMS well velocity at the diffractor location.

This procedure is then carried out for each point along the *true-diffraction curve* to yield the complete response of time migration to a point diffractor. Details of the algebra of this computation are given in the Appendix and the results are shown in Figure 5. In generating this figure we have again used the vertical RMS well velocity that was used in Figure 3. Note that the plume envelope in Figure 4 matches the curve in Figure 5 exactly. Thus the two ways of geometrically constructing the time-migration response to lateral velocity variation are consistent with each other.

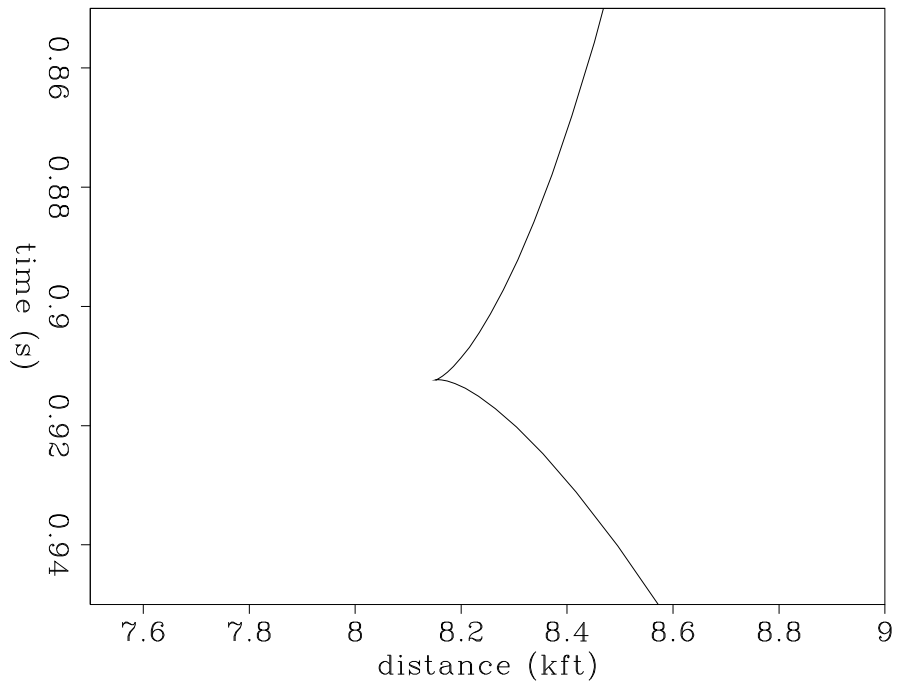

Figure 5: Plume derived by hyperbola summation with the common-tangent construction. This curve corresponds to the envelope of semicircles in Figure 4 exactly. dimitri1-vwell [ER]

KIRCHHOFF MODELING AND MIGRATION

To confirm the geometrical predictions of plumes, we now turn to wave-equation synthetic experiments on point diffractors beneath the lateral velocity variation shown in Figure 1. A Kirchhoff modeling program and a Kirchhoff datuming program are used to generate synthetic data for time migration. The modeling program is similar to Claerbout's `trimo()` routine (1992) except that it incorporates topography. The diffractor response is modeled in two steps:

- The Kirchhoff routine is used to generate the data that would be recorded along the wedge interface where the velocity contrast occurs.

- This synthetic data is then upward continued to the earth's surface using a wave equation datuming program (Bevc, 1992).

The resulting asymmetric diffraction curve is displayed in Figure 6. The kinematics correspond closely to the ray-tracing result shown in Figure 2. The Kirchhoff migrated image in Figure 7 was generated from this diffraction curve using the RMS velocity that would be derived from a well drilled straight down into the diffractor, as before. Note the distinctive plume response evident in this figure. The common-tangent result is superimposed on the migrated image, showing that the agreement between wave-equation results and geometrical predictions is excellent.

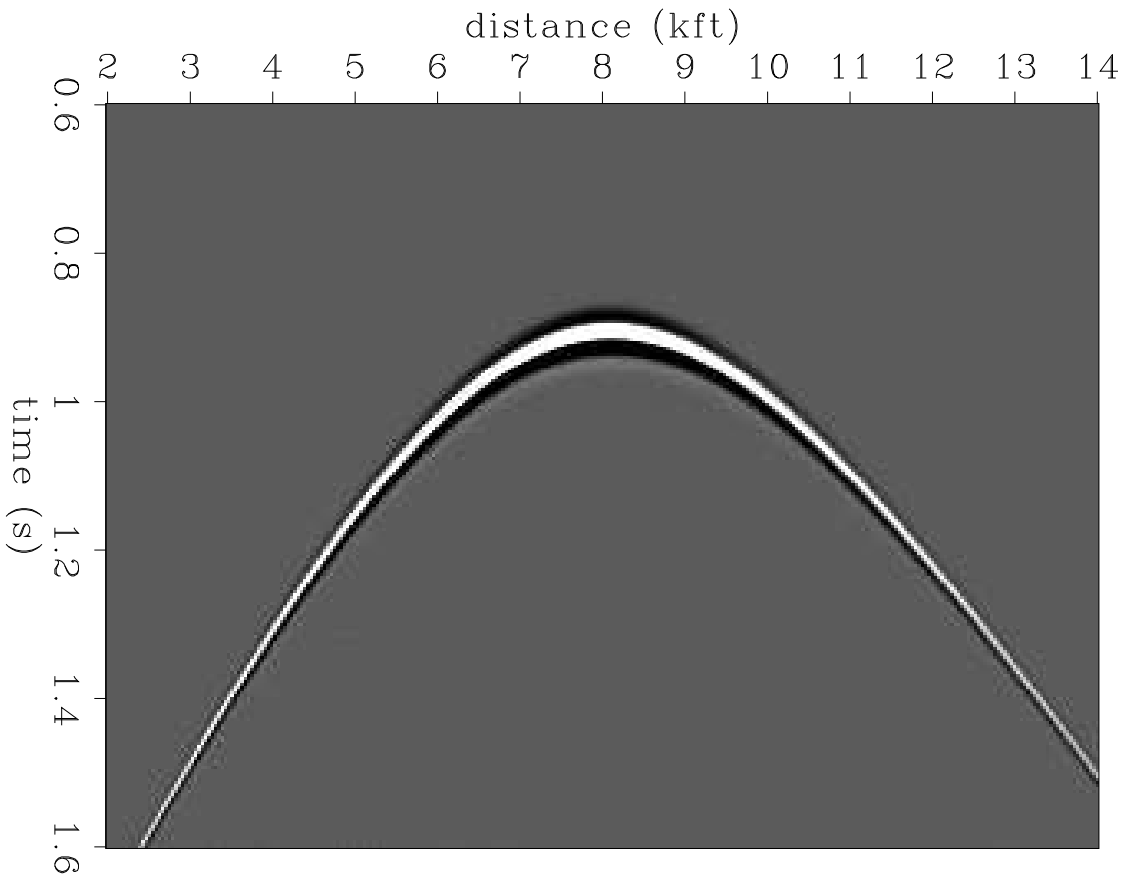

Figure 6: Kirchhoff modeling result for the point diffractor model. The kinematics correspond to the ray-tracing result shown in Figure 2. dimitri1-moddifr [ER]

Zero-Offset Stolt and Gazdag Migration

The wave-equation evidence for plumes in the previous section relied upon the Kirchhoff migration technique, which is very closely related to our geometrical constructions. It is of interest to see whether the plume shape appears when other types of time migration are used. Thus we present Stolt and Gazdag phase-shift migration

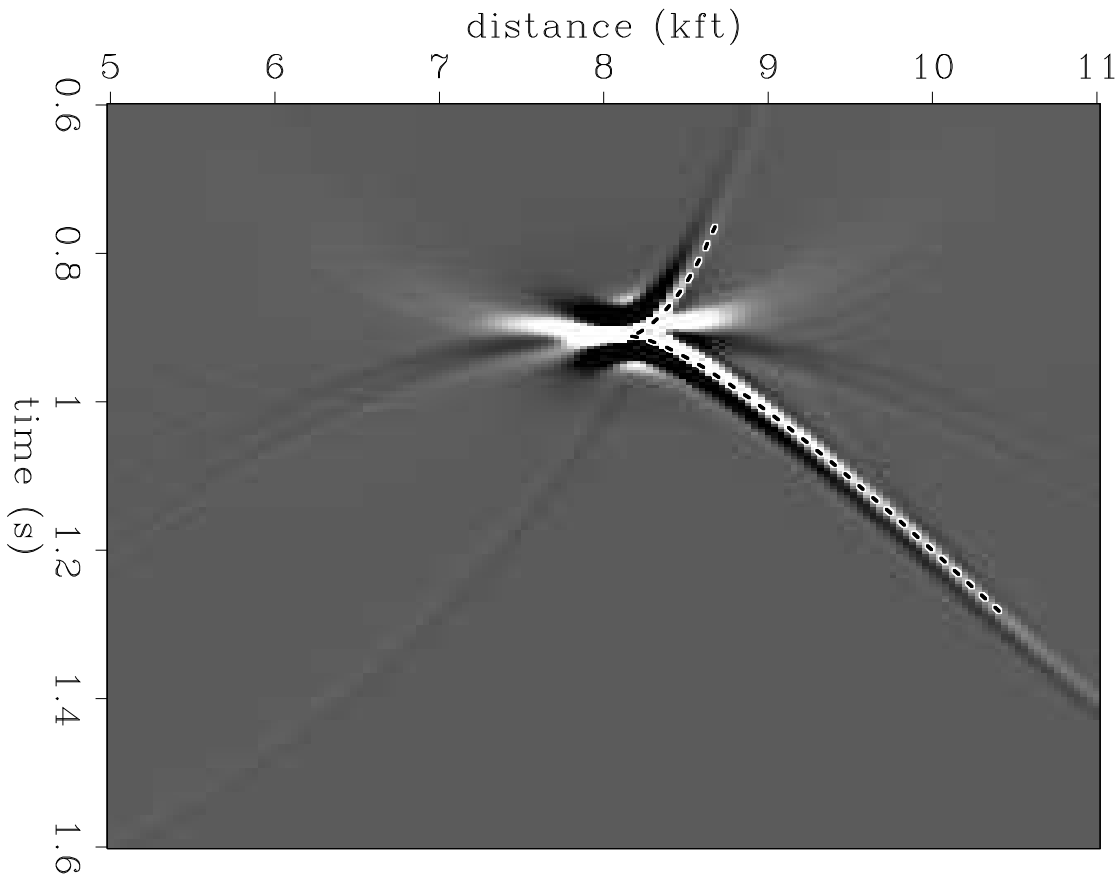

Figure 7: Comparison of the Kirchhoff migration result and the tangent construction. dimitri1-kirch [ER]

images of the point diffractor in Figure 8 and Figure 9 respectively. Both the Stolt and Gazdag results were obtained using a constant RMS well velocity having the same value as in Figure 7. Notice that in both cases we obtain plume shapes that are in good agreement with our geometrical constructions and with the Kirchhoff result of Figure 7.

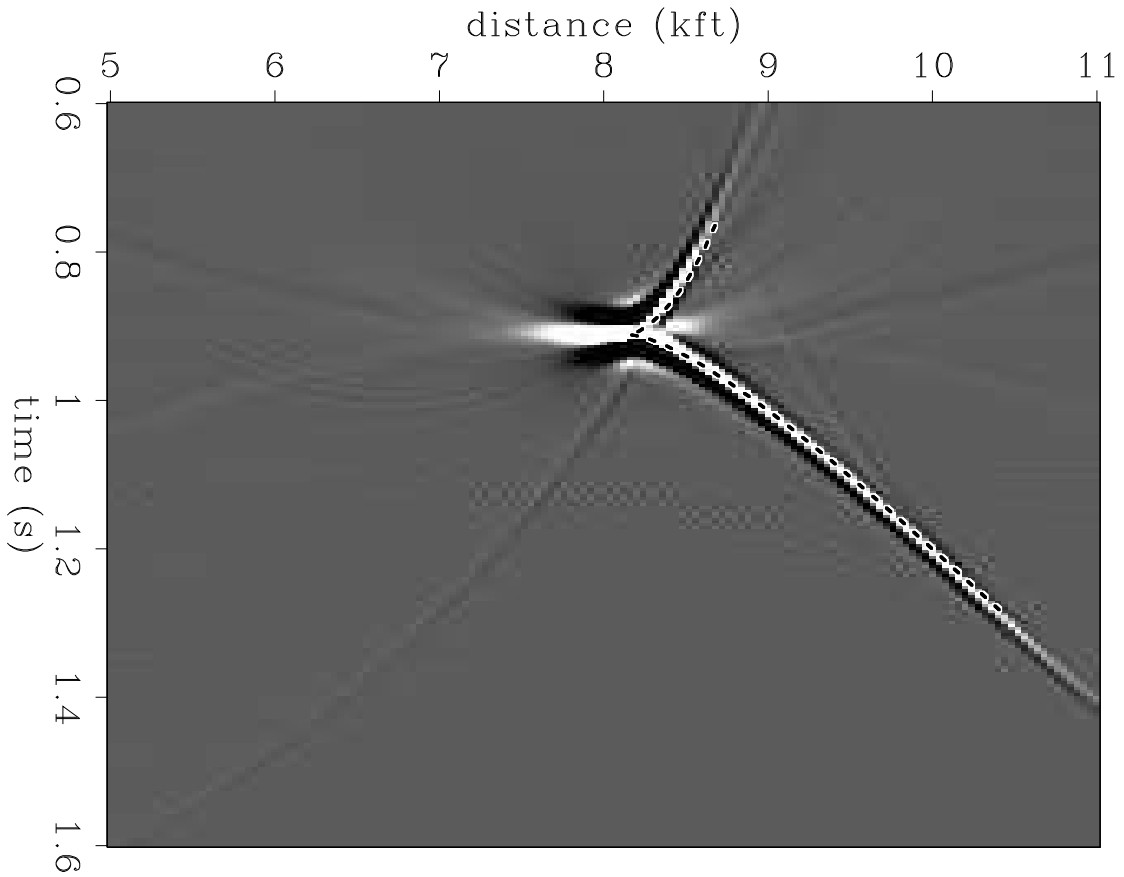

Figure 8: Stolt migration with the common-tangent construction overlaid. dimitri1-stolth [ER]

COMPARISON TO FIRST-ORDER THEORY

Black and Brzostowski (1993) derive simple expressions for the positioning error of time migration. We have used some of their intermediate results in equations(A-4)-(A-6) to calculate the theoretical plume response. In this section we review Black and Brzostowski's first-order theory of plumes and compare it to our previous results.

The geometry used for the derivation of the theoretical result is illustrated in Figure 10. Starting at the point diffractor location (x_m, z_m), a normal ray is traced to the surface where it emerges at x_0. Time migration then translates us to the point x_k. Black and Brzostowski go on from x_k along the image ray to the point Q. The difference between Q and (x_m, z_m) is the error after the image ray correction. Since

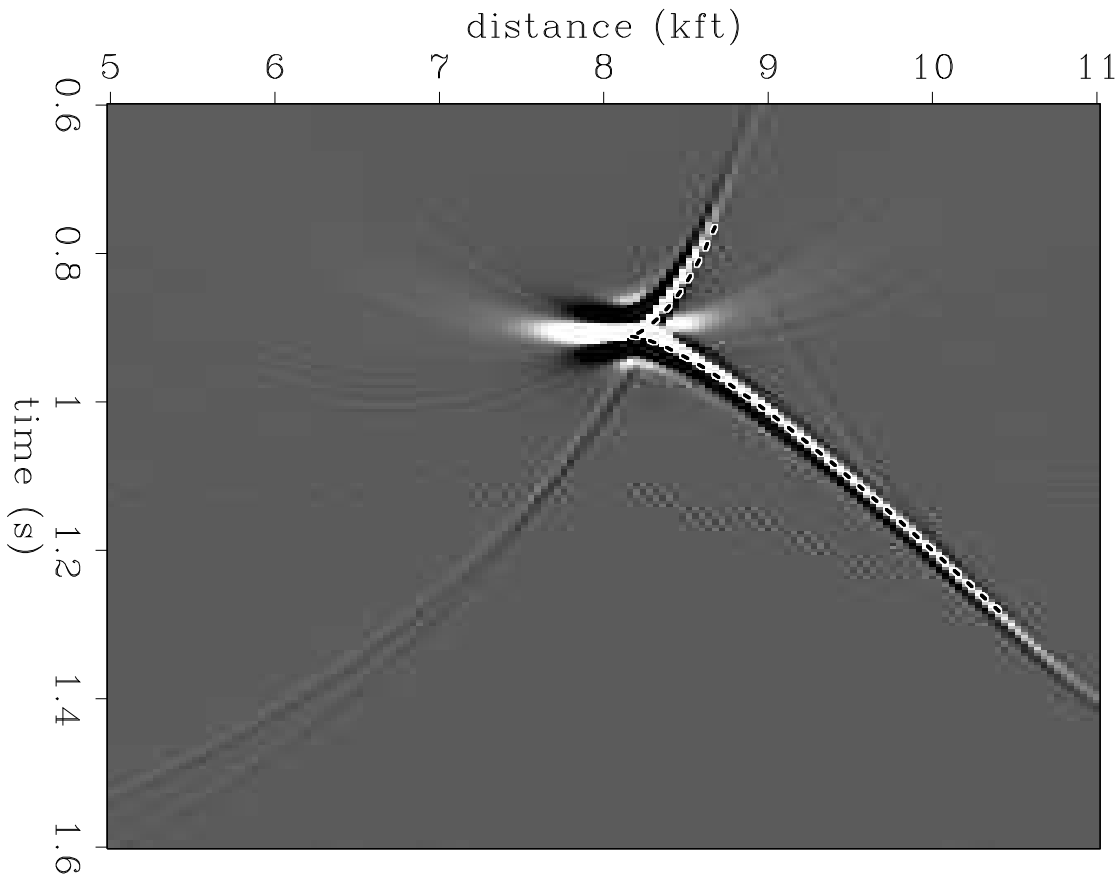

Figure 9: Gazdag phase-shift migration with the common-tangent construction overlaid. dimitri1-gazdag [ER]

we are concerned with the response of time migration to lateral velocity variation, we are interested in the time migrated position (x_k, t_k).

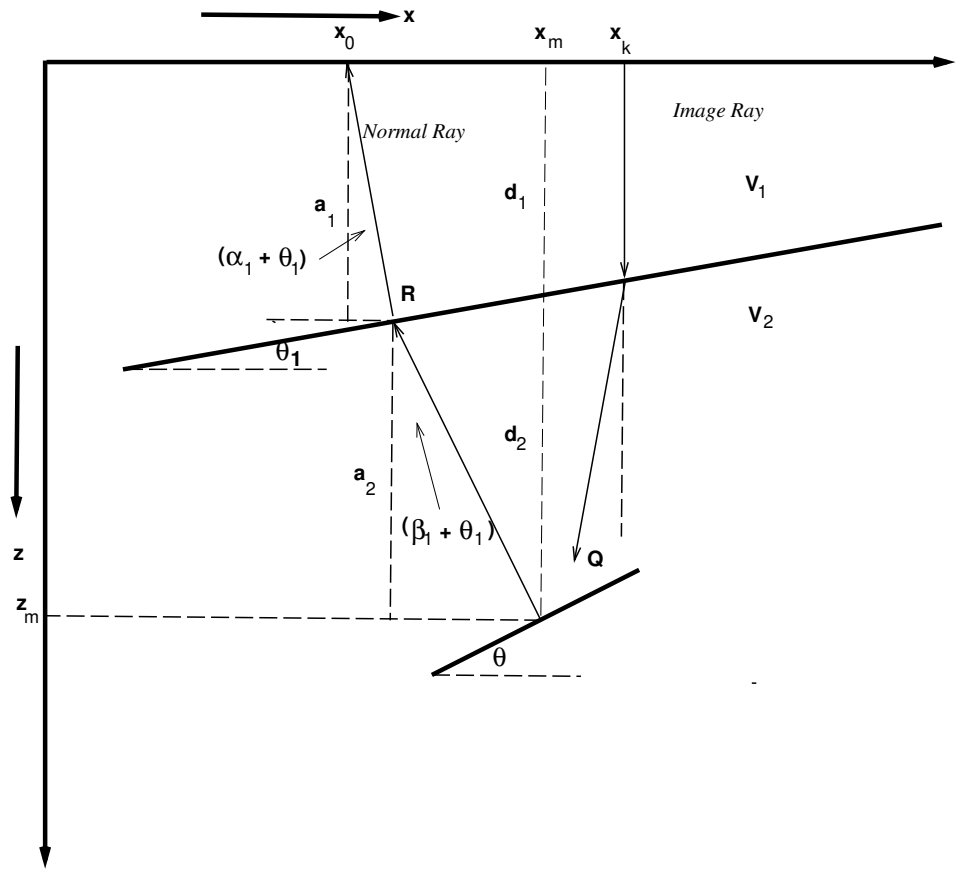

Figure 10: Geometry and raypaths for the dipping layer model. The diffractor is positioned at (x_m, z_m). The spatial and temporal coordinates of the diffraction curve and time migrated image are given by (x_0, z_0) and (x_k, z_k), respectively. dimitri1-fig2 [NR]

The velocity gradient which gives rise to the plumes is due to the velocity contrast across the dipping layer and the dip angle θ_1. To simplify the analysis velocity contrast is defined as:

$$\gamma = \frac{v_2 - v_1}{v_2}$$

The analysis is then carried out to first order in γ and $\sin\theta_1$. This yields the surface location x_0 and travel time t_0:

$$x_0 - x_m \approx -z_m \tan\theta + \gamma d_1 \frac{\sin\theta}{\cos^3\theta} - \gamma \sin\theta_1 z_m \frac{1}{\cos^4\theta} + A\frac{1+\sin^2\theta}{\cos^4\theta} \tag{4}$$

$$\frac{v_2 t_0}{2} \approx \frac{z_m}{\cos\theta} + \gamma d_1 \frac{1-2\sin^2\theta}{\cos^3\theta} + \gamma \sin\theta_1 z_m \frac{\sin\theta}{\cos^4\theta} - 2A\frac{\sin^3\theta}{\cos^4\theta} \tag{5}$$

where the quantity A is defined as

$$A(x_m, z_m) = d_2 \gamma \sin\theta_1 \tag{6}$$

By varying θ, equations(4) and (5) define a diffraction curve like that given in Figure 2. The first term of the equations yields the constant velocity hyperbola, the second term contains the effects of vertical velocity gradients, the third and fourth terms contain the effects of lateral velocity changes.

Time migration is carried out by performing the common-tangent construction. Matching the slope of the hyperbola in equation (1) to the time dip D of the event leads to equations(2) and (3). Expanding these to first order in γ and $\sin\theta_1$ gives the spatial and temporal position of the event after time migration:(Black and Brzostowski, 1993).

$$x_k \approx x_m + A(x_m, z_m)(1 + 3\tan^2\theta) \tag{7}$$

$$\frac{v_2 t_k}{2} \approx \frac{v_2 t_m}{2} - 2A(x_m, z_m)\tan^3\theta \tag{8}$$

We can vary θ in equations (7) and (8) to get a first order analytic representation for the plume. This is done for propagation angles of $\pm 60^\circ$ in Figure 11.

The theoretical result is well positioned relative to the synthetic result. The synthetic plume is skewed upwards whereas the theoretical plume is symmetric about a horizontal axis drawn through its apex. The lower limb of the theoretical plume overlies the synthetic result very closely, however the upper limbs do not match. Both the theoretical and synthetic plume open in the same direction and display the same type of limb curvature: convex upward on the upper limb and convex downward on the lower limb.

Although the first order theory contains some of the features of the plume, it is incomplete. It is clear that a higher-order theory is needed to explain all the features of time migration plumes.

CONCLUSION

A simple theory by Black and Brzstowski predicted that the response of zero-offset time migration to a point diffractor in a `v(x)` medium would be a distinctive cusp-shaped curve called a "plume". We have demonstrated that plumes exist by migration of synthetic data using various time-migration methods. We have also computed the shape of the plumes by two geometrical construction methods. These two geometrical methods compare well and explain the observed migration results. The simple first-order theory explains some of the features of the plume but lacks higher order terms which could account for asymmetry

ACKNOWLEDGEMENTS

The authors would like to thank Lin Zhang and Jon Claerbout for their suggestions and discussions during the SEP summer seminar series. James Black wishes to express

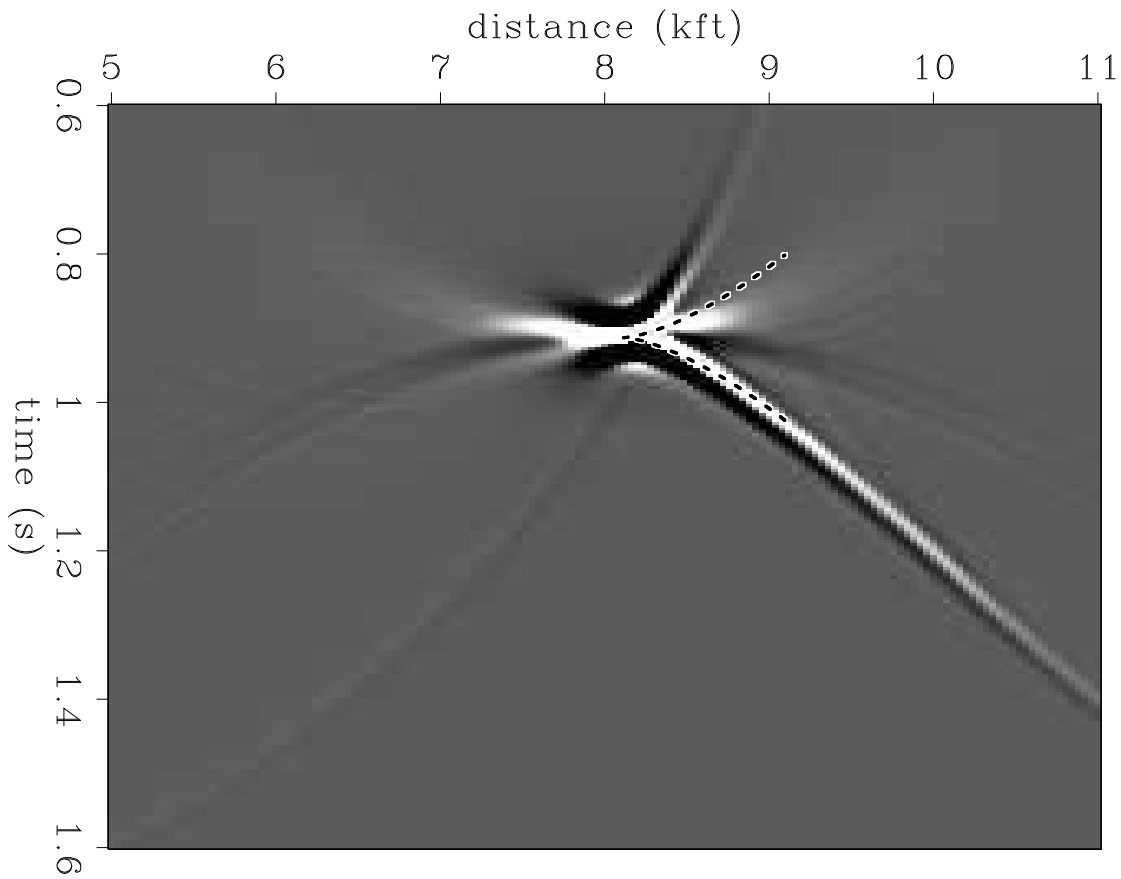

Figure 11: Comparison of the analytic expression for the plume to the Kirchhoff migration result. The migration result is identical to Figure 7, but here we overlay the theoretical result derived by Black and Brzostowski. dimitri1-analytic [ER]

his gratitude to IBM for allowing him to spend time at Stanford during which most of this work was done.

REFERENCES

Bevc, D., 1992, Kirchhoff wave-equation datuming with irregular acquisition topography: SEP–**75**, 137–156.

Black, J. L., and Brzostowski, M. A., 1993, Systematics of time–migration errors: Accepted for publication in Geophysics.

Claerbout, J. F., 1992, Anti aliasing: SEP–**73**, 371–390.

Hatton, L., Larner, K. L., and Gibson, B. S., 1981, Migration of seismic data from inhomogeneous media: Geophysics, **46**, no. 5, 751–767.

Hubral, P., 1977, Time migration - some ray theoretical aspects: Geophys. Prosp., **25**, no. 4, 738–745.

Larner, K. L., Hatton, L., Gibson, B. S., and Hsu, I. C., 1981, Depth migration of imaged time sections: Geophysics, **46**, no. 5, 734–750.

Schneider, W. A., 1978, Integral formulation for migration in two-dimensions and three-dimensions: Geophysics, **43**, no. 1, 49–76.

Yilmaz, O., 1987, Seismic data processing: Soc. Expl. Geophys.

APPENDIX A

In this Appendix, we derive the analytical formulae used to obtain the ray-tracing results for the dipping layer model and the tangent construction migration.

The first step is to model the asymmetric *true-diffraction curve*. This is done by applying Snell's law at the point R where the normal ray crosses the interface in Figure 10. Snell's law at R is given by

$$\frac{\sin\alpha_1}{v_1} = \frac{\sin\beta_1}{v_2} \tag{A-1}$$

where α_1 and $\beta_1 = \theta - \theta_1$ are the angles of incidence at the interface. The vertical distances (a_1,a_2) are expressed in terms of the vertical distances (d_1,d_2) at the migrated position. From the geometry of Figure 10 we get

$$d_1 = a_1 - a_2 \tan\theta \tan\theta_1 \tag{A-2}$$

$$d_2 = a_2 + a_2 \tan\theta \tan\theta_1 \tag{A-3}$$

We now wish to derive the x-displacement along the normal ray. From Figure 10 we see that this is the sum of two terms:

$$x_0 - x_m = -a_1 \tan(\theta_1 + \alpha_1) - a_2 \tan\theta \tag{A-4}$$

the travel time along the normal ray is given by

$$t_0 = \frac{2a_1}{v_1 \cos(\theta_1 + \alpha_1)} + \frac{2a_2}{v_2 \cos\theta} \tag{A-5}$$

The apparent time dip D at the earth's surface is given by

$$D = -\frac{2\sin(\theta_1 + \alpha_1)}{v_1} \tag{A-6}$$

Equations (A-4) and (A-5) define the *true-diffraction curve* (Figure 2).

Common-tangent migration is performed by matching the time dip D (equation (A-6)) with the dip of the *time migration curve* and moving the point to the apex of the *time migration curve*. Carrying out this procedure as discussed in the main text results in Figure 5.